A 10 mA, steady-state, charge exchange negative ion beam source

I. Shikhovtsev [1, 2, a)], V. Amirov[1], K. Anikeeva[1], V. Davydenko[1], I. Emelev[1, 2], A. Ivanov[1, 2], V. Mishagin[1], V. Rashchenko[1, 2], I. Maslakov[1], E. Shubin[1]

[1]*Budker Institute of Nuclear Physics, Novosibirsk, Russia*
[2]*Novosibirsk State University, Novosibirsk, Russia*

[a)]Corresponding author: i.v.shikhovtsev@inp.nsk.su

Abstract. A negative ion source, which utilizes a conversion of primary high current proton beam into negative ions in a gas target via charge-exchange collisions, is under development in Budker Institute, Novosibirsk. The beam is supposed to be used for injection into tandem accelerator, which is a part of the neutron source dedicated for boron-neutron capture therapy. The ion source is designed to produce a beam contains ≥50% of H_2^+ molecular ions. The initial ion beam current is about 1 A at 30 keV energy. After molecular ions dissociation in a gas target, which produces protons with an energy of 15 keV, and further charge-exchange collisions, the beam after target will contain about 2% of negative ion specie with a current in excess of 10mA. The negative ion beam is then separated by the magnetic field, accelerated up to an energy of 105 keV and enters the tandem accelerator. This paper presents the results of simulation of the beam formation, acceleration and transport. The arrangement of the ion source and corresponding high voltage power supply are also discussed.

INTRODUCTION

The surface production [1, 2] or volume production [3] ion sources are widely used to produce the negative ion beams. These methods are well developed and successfully used in many applications. In particular, the methods enabling to reduce the flow of co-extracted electrons from the plasma emitter together with negative ions are applied. The methods of optimal cesium injection into surface production ion source have also been developed [4]. At the same time, the negative ion beam with current of tens of milliamperes can also be produced by charge-exchange of a hydrogen ion beam in a gas or vapor target. A hydrogen beam with energy of 10÷15 keV passing through a gas target contains 2% component of negative hydrogen ions, which can be filtered into a separate beam [5].

The Budker Institute has experience in the development of charge exchange sources of negative hydrogen ion beams for injection into accelerators. In the 70s, at Budker Institute, a pulsed charge exchange source of H^- beam with current of 20 mA and pulse duration of 10^{-4} s was developed [6, 7]. The initial proton beam in this source was formed by a three-electrode multi-slit fine-structure ion-optical system from a plasma jet produced by an arc generator. The formed proton beam with energy of 12 keV and current of ~2 A passed through a pulsed hydrogen target. The H^- beam obtained in the hydrogen target was separated by a magnet and entered an accelerating tube.

In the proposed ion source, the negative ion beam is produced via dissociation of primary molecular ion beam and subsequent charge-exchange in hydrogen gas target. The primary ion beam is formed with an energy two times higher than that corresponds to the maximum yield of negative ions in hydrogen gas target. The ion source has to produce a beam with high H_2^+ molecular ion fraction. They dissociate in the gas target into half energy fragments. An advantage of this method is operation of the plasma emitter in the ion source at low power and low gas pressure in the discharge compared with the sources producing the beams with high content of protons. In this case, continuous operation of the plasma source can be more reliable. An issue would be a separation from high-flux co-streaming positive ions and neutrals, which must be properly disposed onto appropriate beam dumps. In our case, the negative ion beam is deflected by a magnet and then accelerated to an energy about hundred keV. Injection of the beam into the accelerator at high energy enabling a reduction of beam losses at the initial stage of acceleration.

RF ION SOURCE DESIGN

The cut-away view of the negative ion source is shown in Figure 1. The ion source (1) has to provide primary positive ion beam with a current of ~1 A and an energy of 30 keV. The beam passes through the gas target, diaphragm and separation magnet. Inside the vacuum chamber (2) with differential pumping, the positive ion and neutral dumps are placed, as shown in Figure 1. The one gap accelerator (3) is applied to produce 105 keV energy beam. The ion source and vacuum chamber have to be placed on the high voltage platform, which is biased up to -90 kV potential. This provides an acceleration of 15 keV negative ion beam after separation magnet to full energy of 105 keV.

The positive ion source consists of radio-frequency (RF) plasma source and four electrodes ion optical system. In the RF plasma source there is a cylindrical alumina ceramic tube with a Faraday screen installed along the inner cylindrical surface to protect the ceramics from plasma thermal load, sputtering and metallization. The back plate facing the plasma is made of molybdenum. Copper cylinder and molybdenum disc have water cooling though feedthroughs placed on the rear flange of the plasma chamber. Hydrogen gas is puffed into the discharge chamber by using an electromagnetic valve. The ignition unit is placed on rear wall of the plasma source [8].

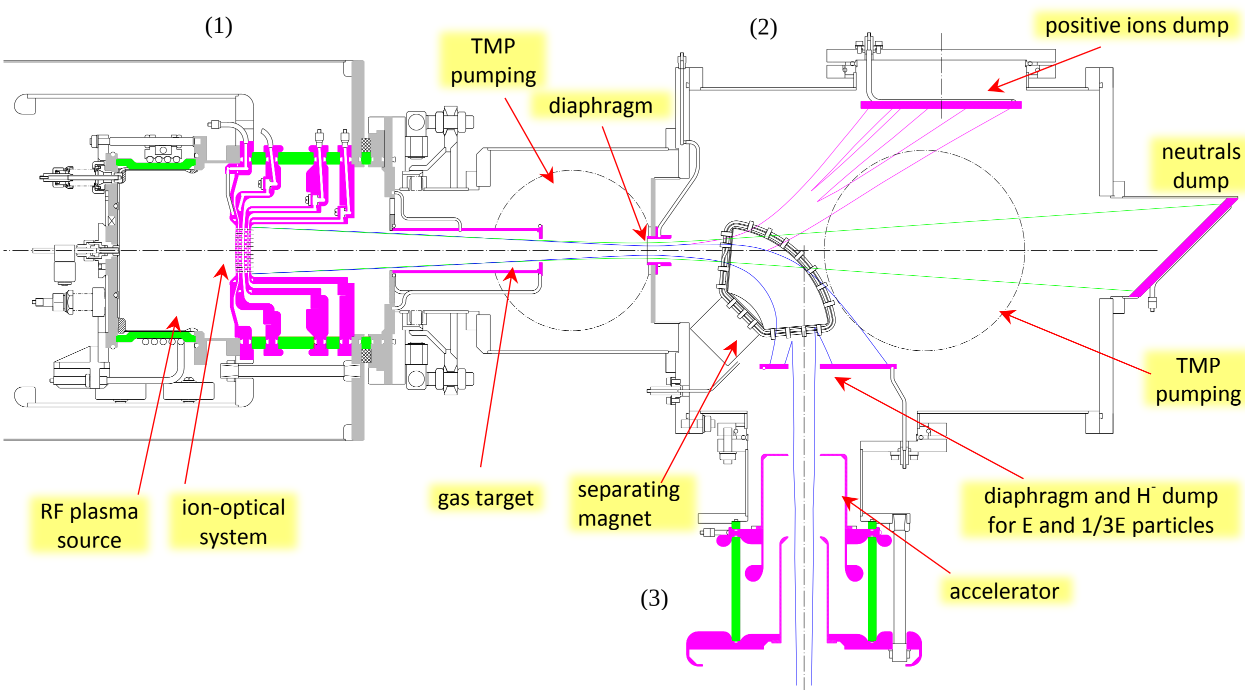

FIGURE 1. Negative ion source design (top view): 1 - ion source, 2 - vacuum chamber, 3 – accelerator.

The four turns RF antenna is wound around the ceramic tube. It is made of 6 mm cooper tubing with heat shrinkable tubing insulation.

The multi-aperture four-electrode ion-optical system is shown in Figure 2. The electrodes have spherical form with radius of 0.5 m for ballistic focusing of the beam. They made of chromium zirconium bronze and have 109 round apertures with diameter of 4 mm arranged in a hexagonal pattern inside diameter of 6 cm. The transparency of the electrodes is about 50%. Each electrode has water-cooling channel surrounding the apertures. Water channels are inside the electrode holders and go out through the flanges compressed between alumina ceramics insulators.

The gas target represents a copper tube with internal diameter of 5 cm and 19 cm long. It has cooling circle line at the output and gas input in the middle part.

The diaphragm splits the vacuum vessel into two volumes for differential pumping. It is made of magnetic steel to avoid penetration of weak stray magnetic field from the separation magnet through diaphragm into left side. This prevents the deflection of the ions in front of the diaphragm. Internal part of the diaphragm is made of copper.

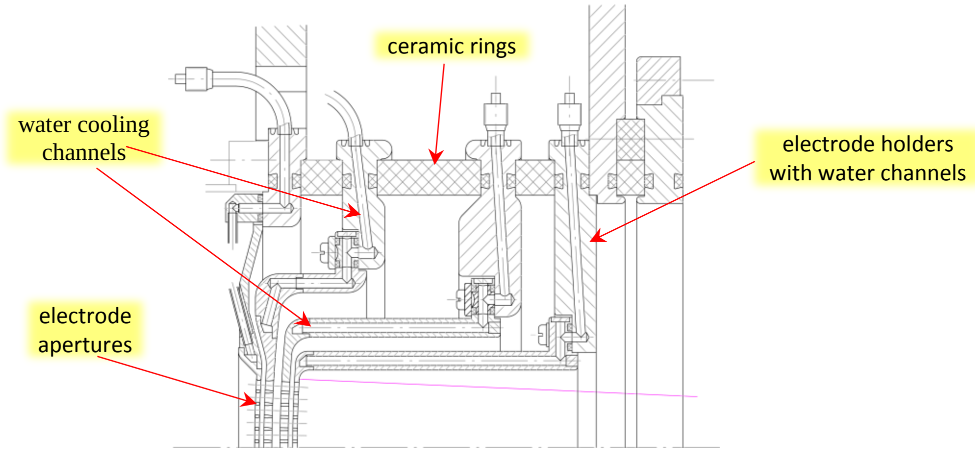

FIGURE 2. Ion optical system.

The separating magnet is designed to deflect the negative ion beam by 90 degrees. General view of the separation magnet is shown in Figure 3. The magnet consists of an open magnetic core with two poles, a set of permanent magnets to create the main magnetic field, overhead profiled poles that create a non-uniform magnetic field for radial focusing of the beam and magnetic field correction coils. The correction coils are made of copper tubs through which water flows for cooling. The field in the central plane of the magnet is 0.175 T. The same magnet was used in the experiments for transportation and acceleration of the negative ion beam for tandem accelerator [9].

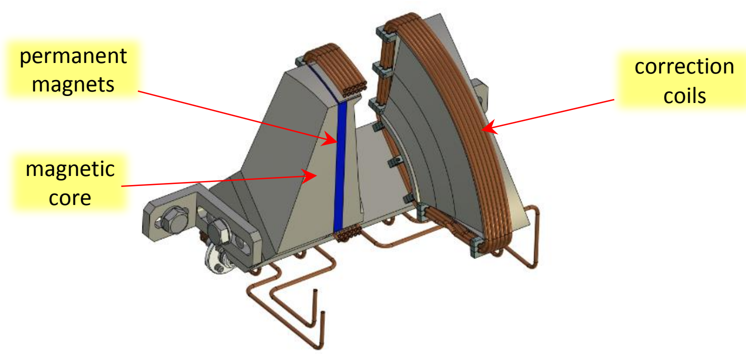

FIGURE 3. Separating magnet.

The water-cooled plate is instilled after the separating magnet. It has a diaphragm for passing through the negative ion beam with energy of 15 keV. The negative ion species with half and one third energy are dumped on the plate.

The accelerator has two copper electrodes with 8 cm apertures separated with alumina ceramic tube. Distance between electrodes is 10 cm. In front of the first electrode, the suppression electrode (not shown) is installed to prevent electrons from entering the accelerator. It is biased under -300 V potential to the accelerator electrode.

The dumps of positive ions and neutrals have to accept high enough power loads. The neutral beam power is 24 kW for initial primary 1 A ion current beam. The beam dump has an inclined surface towards the beam direction to handle this power. The beam dump is still under development.

To reduce the stripping of the negative ion beam, high vacuum is to be provided in the transport region using differential pumping by turbopumps with 1000 and 3000 l/s pumping speed.

SIMULATIONS

The structure of the elementary beam cell and the results of numerical simulations of the beam formation using PBGUNS code are shown in Figure 4. The similar geometry of the elementary cell has been used previously to form a beam for plasma diagnostics in fusion devices [10]. The gaps between electrodes are slightly changed. The thickness of the extraction and acceleration electrodes is changed from 4 to 3.5 mm. The thickness of the plasma grid and ground grid is 2 mm. The gaps are 4.7, 3.5, 2 mm. The circular apertures is 4 mm in diameter. Ion current density is about 65 mA/cm^2. Emittance plot at a distance 2.6 mm from grounded electrode is shown in Figure 5. Maximum beam divergence is about 20 mrad.

The relatively low current density is chosen to generate higher molecular ion fraction. In [11], it is observed that beam current shows a weak dependence of the content of molecular ions H_2^+ from the beam current and, accordingly, from the power in the radio frequency discharge. It was also observed that the content of molecular ions would be about 50% when the ion source operates at low gas pressure. It means that the plasma source can operate at reduced gas puff and an approximately half-reduced RF power in the plasma discharge. The study to increase the content of molecular ions will be continued. In particular, there is an indication that metal surface of the Faraday shield in the plasma box could increase fraction of the molecular ions in the discharge. Note, that in [11] the dependences were obtained with ceramic plasma box wall.

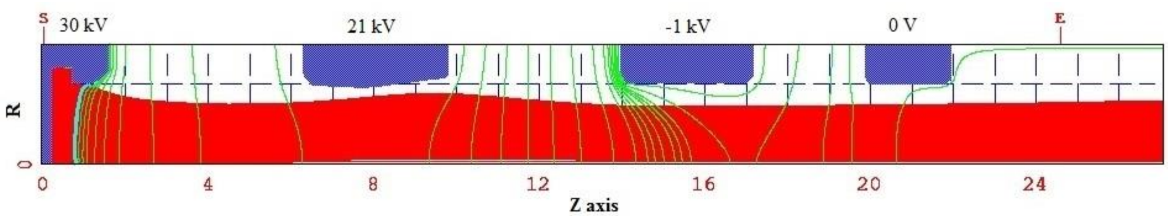

FIGURE 4. Cell geometry with equipotentials and particle trajectories for 30kV accelerating voltages.

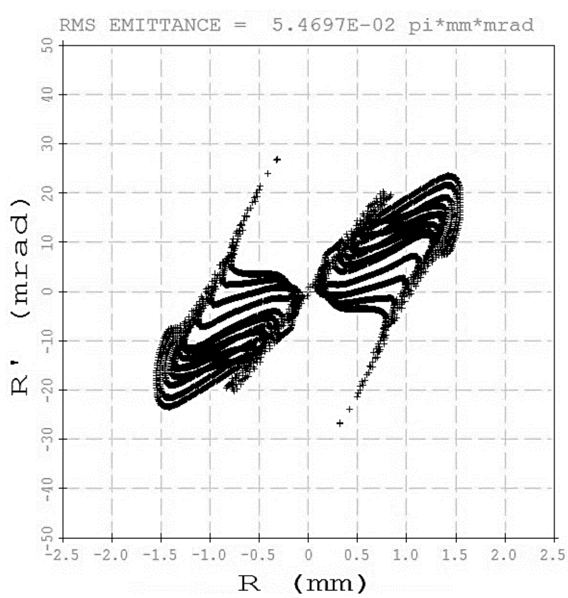

FIGURE 5. Emittance plot.

The simulation results of the beam transport through diaphragm, separation magnet and acceleration system are shown in Figure 6. The beam starts from an ion-optical system with a focal length of 50 cm. The diaphragm is installed in the beam waist area. After that, the beam expands and enters the magnet. A non-uniform magnetic field of the magnet focuses the beam and directs it to the accelerator. At the exit of the accelerator, the beam is focused and has a round shape (Figure 7).

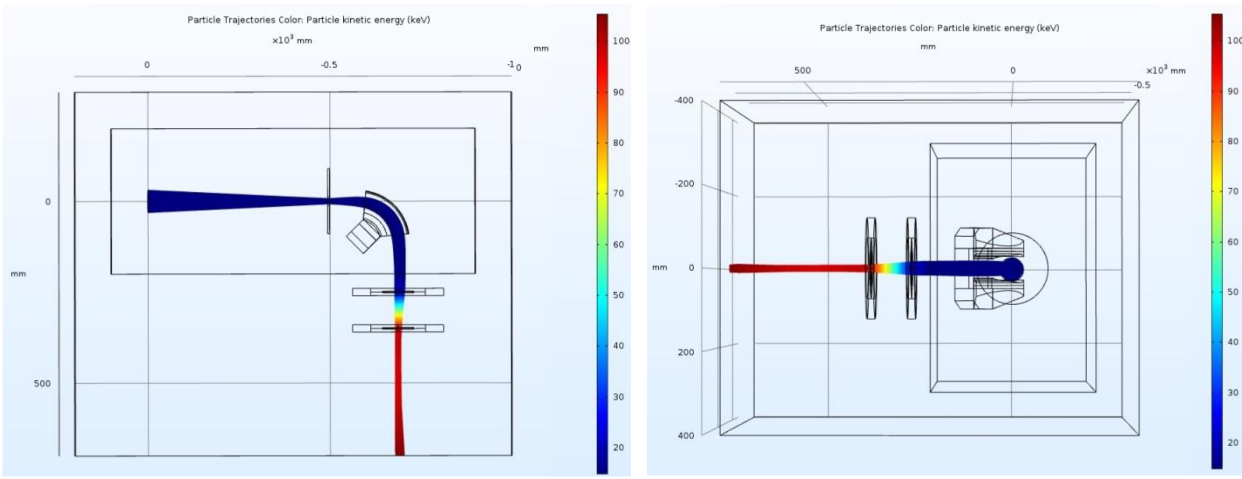

FIGURE 6. Trajectories of the negative ions beam with an energy of 15 keV: top view (left), view towards the primary beam (right).

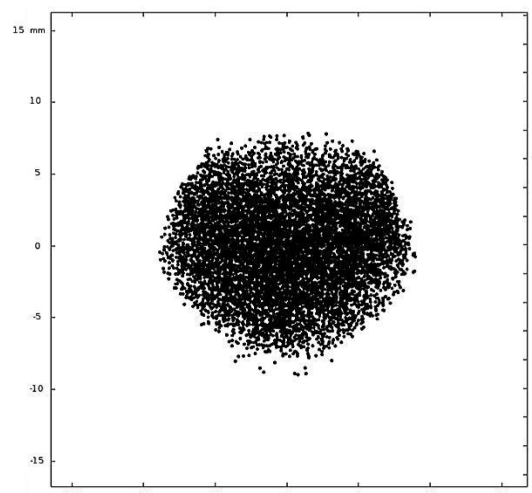

FIGURE 7. Beam cross section at a distance of 30 mm after the accelerator.

The simulation results of the trajectories of residual fast atoms and protons are shown in the Figure 8. There are the positive and negative fractions of the beam with the full energy, as well as with the energies 1/2 and 1/3 of the full, obtained as a result of charge-exchange and dissociation of the primary ion beam in the gas target. Since these fractions contain significant power, they must be directed onto special water-cooled dumps.

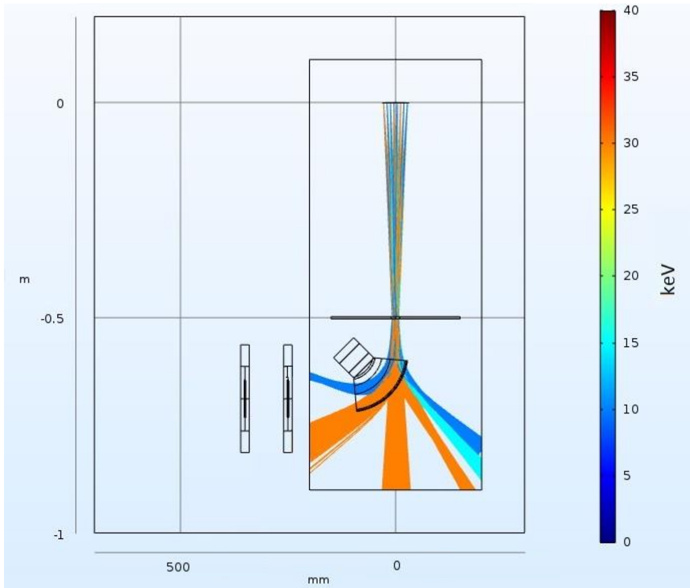

FIGURE 8. Trajectories of the other beam components: neutral beam on the center, positive ions – right side, negative ions – left side.

The results of the simulation of vacuum conditions and the gas puffing system show that in order to comply with the optimal conditions for plasma generation in the RF box, the gas puffing into the plasma box should be about 0.6 mbar·l/s.

The dissociation cross section for particles with an energy of 30 keV is $\sigma = 1.9 \cdot 10^{-16}$ cm^2. In order to have the gas target to be "thick", the $\sigma \cdot n \cdot l$ should be ~5. This can be achieved at a target density of $1.4 \cdot 10^{15}$ cm^{-3}, or 0.05 mbar. To create the required pressure, additional gas puff into the gas target is provided with flow rate about 1 mbar ·l/s.

Passing through the gas target, the half-energy particles will have a larger angular spread than was in the initial beam. Additional angular spread is caused by the process of dissociation and scattering. Additional broadening should be no more than 0.5° according to the results of optical measurements of the angular spread of the beam components with an initial energy of 50 keV which were done in [12]. The angular spread of the component with energy of E/3 is 0.4° larger than the angular spread of the full energy component. Additional angular spread will lead to the loss of a part of the beam, which is not significant, since there is a current margin. At primary ion beam current of 1 A, the maximum current of the negative ion beam from the gas target should be about 14 mA. This value is higher than that required for the BNCT accelerator.

RF POWER SUPPLY SYSTEM

The RF power supply system (Figure 9) is designed to apply power to the plasma source. It consists of a radio frequency generator (RFG), matching network and high voltage isolation transformer. The load is plasma emitter with antenna and capacitors connected to the antenna outputs. RFG is configured as a modular system consisting of the four RF modules based on semiconductors, combiners of the first and second stage, RF control module. The industrial power source 15 kW TDK-Lamda is used as DC power supply. The output RF power is 9 kW. The output impedance of the RFG is 50 Ohms.

The matching network consists of fixed capacitor and inductance and is designed to maximize power transfer from a 50 Ohm RF power source to the load with the different impedance values.

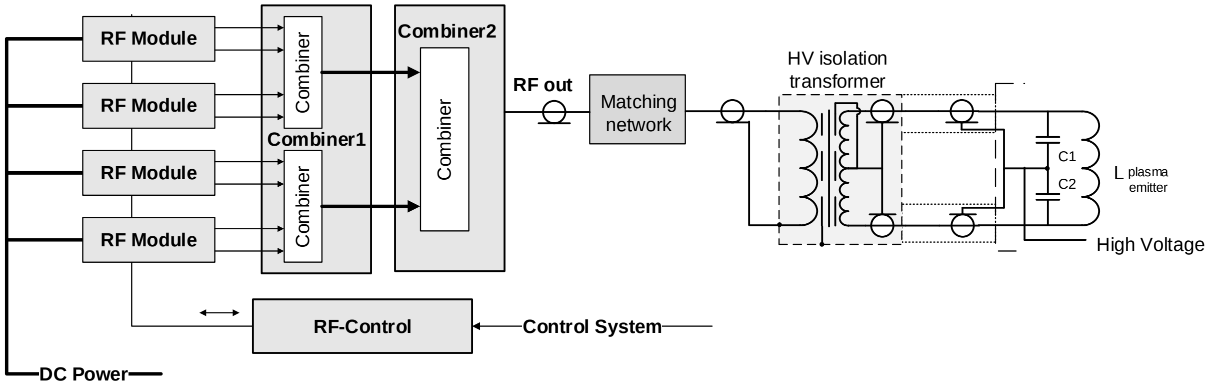

FIGURE 9. Schematic of the RF power supply system.

In this case, the load is high voltage isolation transformer and plasma emitter – RF antenna inductance and plasma impedance. Isolation transformer decouples the RF generator and the plasma source, which is at high potential (30 kV). The transformer is made from high voltage RF cable with solid and oil insulation. It has ferrite core.

HIGH VOLTAGE POWER SUPPLY

Figure 10 shows the functional diagram of the high voltage power supply (HVPS) of the accelerating and extracting grids of the injector. The HVPS is designed for continuous operation. The maximum output power is 75 kW. The output voltage is regulated within 3 ... 30 kV, the maximum output current is 2.5A. The HVPS is designed according to the current loop topology. The primary rectified mains voltage is applied to 6 identical inverters, which convert it into rectangular alternating current with amplitude of 35A. All inverters operate synchronously and in phase. The output of each inverter forms a galvanically isolated current loop through 15 toroidal transformers of the high voltage rectifier sections. Thus, the total loop current is equal to the sum of the currents from each inverter.

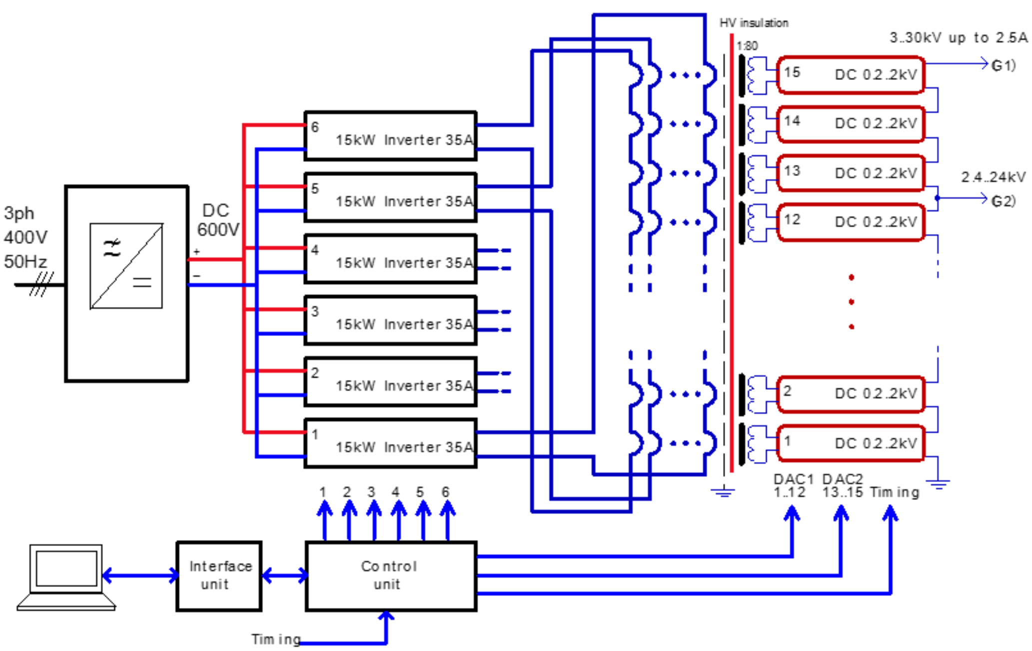

FIGURE 10. Schematic of the RF power supply system.

The secondary winding of each transformer in the high-voltage section has 80 turns. The output rectifier consists of 15 identical sections. Each section has its own voltage regulator and stabilizes the output voltage according to the DAC within 0.2 ... 2 kV. The section outputs are connected in series. To supply the injector extracting grid (G2), an additional output is made from 12 section. To adjust the extracting voltage, the G1 and G2 voltages are separately regulated.

CONCLUSION

Here the design overview of the RF charge-exchange negative ion source is presented. The simulation results shows that the negative ion beam with current of about 10 mA or higher and beam energy of 105 keV can be produced from the primary hydrogen positive ion beam with a current of 1 A and content of molecular ions H_2^+ about 50%. Additional experiments are planned to study the composition of hydrogen ions in the primary ion beam in order to increase the content of H_2^+ molecular ions. The main power supplies (RF PS and HVPS) were designed and manufactured. The ion source is being assembled. In the near future, it is planned to start the experiments.

ACKNOWLEDGMENTS

Reported simulation results of the beam formation, acceleration, transport and other calculations was funded by RFBR, project number 20-32-90053. The designing works, equipment purchase and manufacturing are partially funded by ……ссылка на РНФ…

REFERENCES

1. A.Sanin, Yu.Belchenko, I.Gusev, A.Ivanov, V.Rashchenko, V.Savkin, I.Shchudlo, I.Sorokin, and P.Zubarev, AIP Conference Proceedings **2052**, 050012 (2018); https://doi.org/10.1063/1.5083766.
2. D.Faircloth, S.Lawrie, New J. Phys. **20** 025007 (2018).
3. M.Bacal, A.Hatayama, J.Peters, IEEE Transactions on Plasma Science **33**, No. 6 (2005).
4. Yu. Belchenko, G. Abdrashitov, P. Deichuli, A. Ivanov, A. Gorbovsky, A. Kondakov, A. Sanin, O. Sotnikov, I. Shikhovtsev, Review of Scientific Instruments **87**, 02B316 (2016); doi: 10.1063/1.4932583.
5. C.F.Barnett, J.A.Ray, E.Ricci et al, *Atomic data for controlled fusion research* (Oak Pidge National Laboratory, Oak Pidge, 1977), pp. A.6.2–A.6.3.
6. G.I.Dimov, G.V.Roslyakov, Instruments and Experimental Techniques, No 2, pp. 33-35 (1974).
7. Yu.I. Belchenko, V.I.Davydenko, P.P.Deichuli, et al, PHYSICS-USPEKHI **61**, No 6, pp. 531-581 (2018) DOI: 10.3367/UFNe.2018.02.038305
8. I.V.Shikhovtsev, G.F.Abdrashitov, Yu.I.Belchenko et al, AIP Conference Proceedings **2052**, 040016 (2018); https://doi.org/10.1063/1.5083750
9. A.Sanin, G.Abdrashitov, Yu.Belchenko, A.Ivanov, A.Gmyrya, and L.Perepelkin, AIP Conference Proceedings 2052, 050011 (2018); https://doi.org/10.1063/1.5083765.
10. A.A.Ivanov, V.I.Davydenko, P.P.Deichuli, A.Kreter, V.V.Mishagin, A.A.Podyminogin, I.V.Shikhovtsev, B.Schweer, R.Uhlemann, Rev. Sci. Instruments **71**, 3728-3735 (2000).
11. A.A.Ivanov, I.V.Shikhovtsev, A.A.Podyminogin, I.I.Averboukh, T.D.Akhmetov, V.I.Davydenko, and P.P.Deichuli, Plasma Physics Reports **28**, No.3, pp. 196–203 (2002).
12. A.Listopad, J.Coenen, V.Davydenko, A.Ivanov, V.Mishagin, V.Savkin, B.Schweer, G.Shul'zhenko, R.Uhlemann, Rev. Sci. Instruments **83**, Issue 2, 02B707 (2012).